International Journal of Pharmaceutics 374 (2009) 82–89

Contents lists available at ScienceDirect

International Journal of Pharmaceutics

journal homepage: www.elsevier.com/locate/ijpharm

Modeling and prediction of cocrystal phase diagrams

Abigail Ainouz[a], Jean-René Authelin[a], Pascal Billot[a,*], Harvey Lieberman[b]

[a] Sanofi-aventis, Research and Development, Physical Quality, 94403 Vitry-sur-Seine, France
[b] Sanofi-aventis, Research and Development, Physical Quality, Bridgewater, NJ, USA

ARTICLE INFO

Article history:
Received 4 December 2008
Received in revised form 6 March 2009
Accepted 10 March 2009
Available online 24 March 2009

Keywords:
Cocrystals
Crystal engineering
Pharmaceuticals
Phase diagram
Solubility
Thermodynamics

ABSTRACT

In this paper, a new approach to model cocrystal phase diagrams is presented. Starting from an initial set of data, the phase diagram is obtained from discontinuous isoperibolic thermal analysis (DITA) and basic thermodynamic data (enthalpies and solubilities). The solubility product constant may then be determined. Since this constant is solvent independent, extrapolation to other solvents is possible. Application of this technique to an active pharmaceutical ingredient and glutaric acid demonstrates good agreement between calculated and experimental data.

1. Introduction

The pharmaceutical industry is currently facing more issues than ever in developing new active substances. The development of a new active pharmaceutical ingredient (API) is faced with challenges at the selection of active form, manufacture and storage. Some solids exhibit many polymorphs or hydrates; moreover many APIs are poorly soluble and therefore poorly bioavailable. In recent years, advances in crystal engineering have motivated research in the design of pharmaceutical cocrystals (Zaworotko and Moulton, 2001; Zaworotko et al., 2003a, 2005; York et al., 2007; Aakeröy and Salmon, 2005; Aakeröy et al., 2006). The development of pharmaceutical cocrystals might offer advantages over the API and may overcome some of the limitations encountered with classical salt formation strategy:

- Contrary to salts which require an ionic group and a minimum p*K*a difference of two units between the base and acid, cocrystallization features a complexation between neutral molecules (Variankaval et al., 2006; Bishop et al., 2004). It therefore provides opportunities for more API solid forms. The number of acids and bases that are acceptable for use in pharmaceutical salt formation is limited but there is a wide range of potential cocrystal formers (or co-formers) that may be used to prepare cocrystals (Jones et al., 2006).
- Recent studies revealed that most of the cocrystals of caffeine and theophylline are physically stable at increased relative humidities and demonstrate less of a propensity for hydratation (Jones et al., 2005, 2006; Zaworotko et al., 2003b; Smith et al., 1997).
- Remenar showed that cocrystals of triazole-diacids have greater solubility and faster dissolution properties, similar to amorphous compounds (Remenar et al., 2003). Most importantly, from the numerous strategies existing for enhancing the bioavailability of low soluble drugs, cocrystallization appears to be among the most viable (Mc Namara et al., 2006; Bak et al., 2008)).

In practice, however, there are challenges in screening for cocrystals and their subsequent scaling-up. Currently, various techniques are employed to prepare cocrystals including slow evaporation, slurrying of suspensions, crystallization by cooling and the co-grinding method. The co-grinding method involves mixing two solids together in a mill, optionally with a very small amount of solvent (solvent drop grinding), to induce cocrystal formation through mechanochemistry (Jones et al., 2005, 2002; Braga and Grepioni, 2005). Although this is recognized as one of the most efficient methods for preparing cocrystals, scaling-up is not always obvious (Chiarella et al., 2007).

Slow cooling the cocrystal components from solution remains the most industrially-preferred process, even though there is the risk of crystallizing the single component phases. Thus numerous experimental conditions have to be tested in the laboratory, and scaling-up the crystallization process becomes difficult

* Corresponding author.
E-mail address: pascal.billot@sanofi-aventis.com (P. Billot).

0378-5173/$ – see front matter © 2009 Elsevier B.V. All rights reserved.
doi:10.1016/j.ijpharm.2009.03.016

Table 1
Variance analysis in cocrystal phase diagram zones.

Number of phases	Variance	Description
1	$v = 3$ ($v' = 2$)	Zone 6 is a homogeneous liquid phase. The composition can vary everywhere in the area (geometric dimension = 2 = v'). In a prismatic diagram, incorporating the temperature as a *z*-axis, the composition varies continuously in a volume (dimension = $v = 3$).
2	$v = 2$ ($v' = 1$)	Zone 2: Pure solid API in equilibrium with the liquid containing API whose composition varies along the segment I-K constituting the border between zones 2 and 6 (geometric dimension = 1 = v'). In a prismatic diagram, incorporating the temperature as a z axis, the liquid composition varies continuously on a surface (dimension $v = 2$). Zone 3: Pure solid co-former in equilibrium with the liquid containing co-former whose composition varies along the segment constituting the border between zones 3 & 6 Zone 1: Pure solid cocrystal in equilibrium with the liquid. The liquid composition varies on a curved line between zone 1 and 6.
3	$v = 1$ ($v' = 0$)	Zone 4: pure solid API and pure solid cocrystal are in equilibrium with a fixed liquid composition at point I, which is the intersection of the API/liquid and cocrystal/liquid equilibrium lines (geometric dimension = 0 = v'). In a prismatic diagram, incorporating the temperature as a z axis, the composition of the liquid varies continuously on a line (dimension = $v = 1$). Any point in zone 4 is a heterogeneous mix of the 2 solids and the fixed liquid. Zone 5: pure solid co-former and solid cocrystal are in equilibrium with a fixed liquid composition at point J, which is the intersection of the co-former/liquid and cocrystal/liquid equilibrium lines.

(Rodriguez-Hornedo et al., 2006a; Zhang et al., 2006). To this end isothermal phase diagrams of cocrystal-forming systems are very useful in reducing the number of experiments and can help explain the success rate of solvent drop-grinding experiments (Chiarella et al., 2007).

To determine ternary phase diagrams, earlier methods involved analyzing both the liquid and solid phase (after drying) for each composition. These analyses are quite tedious, extremely time consuming and generally incomplete. For example, HPLC analysis leads to the solid–liquid equilibrium and not the whole phase diagram with multiple stoichiometries.

In this article, we propose an alternative strategy:

1. Acquire the phase diagram from a selected solvent using discontinuous isoperibolic thermal analysis (DITA), a method which has already been established for diastereoisomeric resolution (Marchand et al., 2004).
2. Using the experimental data obtained from a single solvent, the behaviour in other solvents may be estimated by using a generalized form of the thermodynamic complexation/reaction approach already developed by several authors (Ito and Sekiguchi, 1966; Rodriguez-Hornedo et al., 2006b).

Phase diagrams for numerous solvents may therefore be deduced at a reasonable accuracy from a minimal number of experiments. This approach provides valuable information that may be used to develop a crystallization process for a particular cocrystal.

2. Phase diagrams

As much of this paper covers the experimental determination and theoretical calculation of phase diagrams, some details of ternary phase diagrams will be explained.

Ternary mixes can easily be represented using triangular diagrams. In most cases equilateral triangles are used. Any composition may be represented by a point in the triangle, whose composition can be read by projecting the point to the triangle's side.

Triangular diagrams have been used by several authors (Li et al., 2008; Chiarella et al., 2007; Marchand et al., 2004) for the representation of ternary isothermal phase diagrams for API, co-former, and cocrystal in a particular solvent system. A typical phase diagram for a 1:1 cocrystal is represented in Fig. 1. Triangular diagrams are isothermal slices for prismatic diagrams, where the *z*-axis represents the temperature.

This phase diagrams illustrates:

- Three chemical constituents: the API, the co-former and the solvent.
- Four phases: the liquid (solvent dissolving variable quantities of API and co-former), the crystalline API, co-former and cocrystal.

The Gibbs rule of phases allows us to understand the construction of the phase diagram.

$v = c + 2 - \Phi$
v: variance
c: number of independent components
Φ: number of phases
2 refers to the external parameters: pressure and temperature

As there are three components, and one stoichiometric relationship (API + co-former → cocrystal), the number of "independent" components is only 2, therefore:

$$v = 2 + 2 - \Phi = 4 - \Phi$$

If we work in isothermal conditions, we can reduce the number of degrees of freedom by one, and the "isothermal variance" $v' = 3 - \Phi$.

Applying the variance rule to the phase diagram, we arrive at the summary in Table 1.

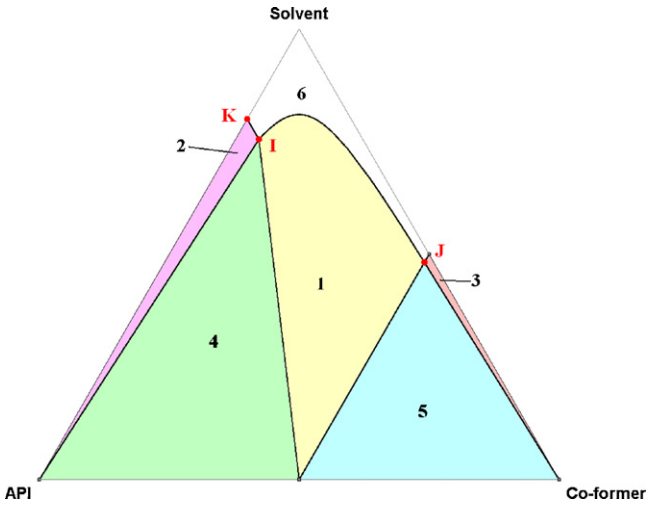

Fig. 1. Typical cocrystal phase diagram.

The points I and J are so called "invariants". In the racemic resolution literature they have also been referred to as "eutectic", by analogy to the eutectic compositions of binary phase diagrams (Collet et al., 1981).

3. Materials and methods

3.1. Acid and solvents

All the reagents were of analytical grade. Glutaric acid and methyl tert-butyl ether (MTBE) were purchased from Acros Organics (Geel, Belgium). Ethyl acetate (AcOEt) was provided by SDS-CARLO ERBA (Val de Rueil, France), acetonitrile (ACTN) by Merck (Darmstadt, Germany), and methyl isobutyl ketone (MIBK) by VWR Prolabo (Fontenay-sous-Bois, France).

3.2. Active pharmaceutical ingredient

An active pharmaceutical ingredient (API) currently in development within Sanofi-Aventis was chosen as a test material.

3.3. Cocrystal (1:1 glutaric acid:API)

The following procedure was used to obtain the first cocrystals after a solvent drop co-grinding screen. 100 g (0.201 mmol) of glutaric acid co-former, and 27.2 g of API (0.206 mmol) were dissolved in 430 mL acetonitrile at reflux temperature (88 °C) in an agitated laboratory glass vessel. The solution was cooled to 54 °C and seeded with cocrystals obtained by a previous synthesis. The mixture was cooled to −10 °C over 2 h 30 min, while stirring continuously. The resulting crystallized solid was filtered and then dried under vacuum overnight. The yield was 92% (116.5 g). Collection of experimental X-ray powder data and comparison to starting materials confirms the formation of a new species.

3.4. DITA

A complete description of the DITA technique, modelling of the signal, and data treatment have already been presented (Marchand et al., 2004).

3.4.1. Principle

The DITA method is a calorimetric method. The principle of the method is to dilute a suspension of one or two solids by adding pure solvent, and to measure the thermal response of the system.

The measuring cell is immersed in water kept at a constant temperature (25 °C) by a surrounding jacket, protected itself by an insulating foam. Agitation is carried out using a magnetic stirrer and solvent is added by a pump (MCP CPF IP65, Ismatec). The computer is connected to the pump to regulate each addition of solvent and also the temperature of the cell (Fig. 2a).

The system to be studied is set under isoperibolic conditions (temperature surrounding the system is held constant) at 25 °C. Starting from a system in thermal equilibrium, a fast injection of small amount of pure solvent, conditioned exactly at the same temperature, is performed. Typically the starting point will be a point chosen on the ternary diagram corresponding to a suspension of two solids: API (or co-former) and cocrystal with enough solvent to provide sufficient stirring. The injection of pure solvent leads to the evolution of the system via dissolution and/or dilution. These phenomena lead to heat exchanges (corresponding to enthalpy changes as pressure is constant) involving temperature variations. The temperature is recorded using a very accurate thermometer with a resolution down to $\pm 10^{-3}$ K. The temperature variations are then plotted versus time. A typical temperature variation versus time curve is presented in Fig. 2b.

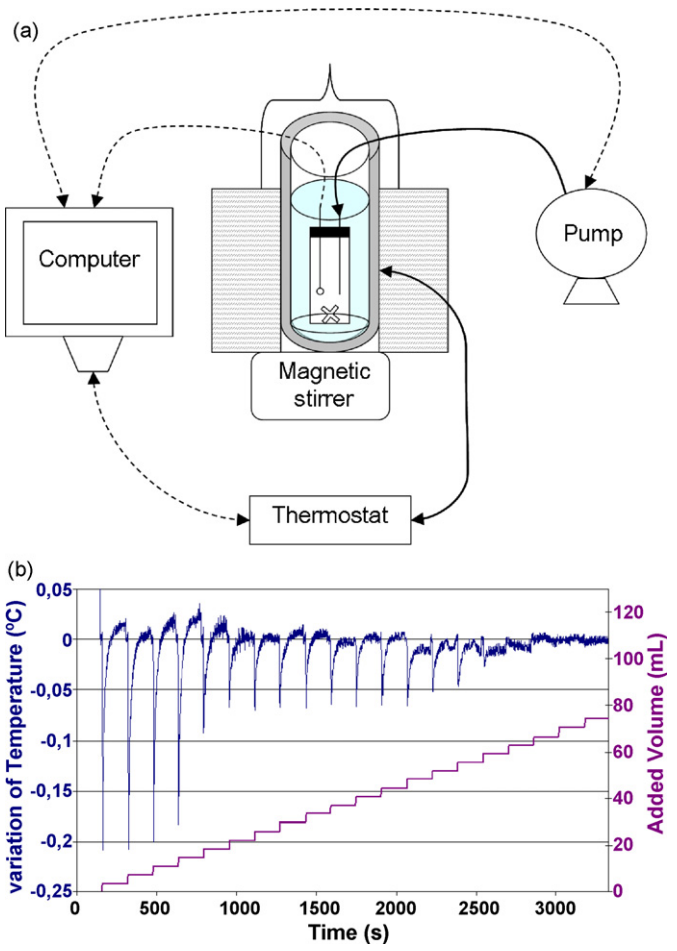

Fig. 2. (a) Experimental setup for DITA. (b) Typical acquisition curve.

The injection provokes a temperature shift proportional to the dissolution enthalpy (as the injection is fast, the temperature rise is close to the adiabatic temperature rise) of the solids in suspension. Then the temperature returns to the baseline due to the response of the thermostat which is not adiabatic.

A typical analysis requires a few grams of the samples and lasts 8–12 h. The process is completely automated with Labworldsoft (IKA, Staufen, Germany). Data are imported to Microsoft Excel for treatment, and all the diagrams are traced on ProSim (Labege, France).

An entire experiment is composed of several injections of solvent (typically 10–20) and therefore several temperature variation versus time curves, as shown in Fig. 2b, are obtained. The cumulated integration values versus the cumulated injection volumes may be plotted as in Fig. 3a. On such a plot, changes in slope are related to the intersections between the limits on the corresponding phase diagram (Fig. 3b), as will be explained in the following section.

A typical example is outlined in Fig. 3b. The experiment starts with a suspension corresponding to point A, in zone 4. The composition at point A is a mixture of pure solid API and solid cocrystal and a liquid of the composition of point I in Fig. 1. When adding pure solvent, the composition of the system follows the dilution line from A to the solvent corner of the triangle (infinite dilution). This trajectory intersects three zones (4, 1, 6) and two borders (points B and C).

Between points A and B, the added solvent will dissolve both the API and the cocrystal. As in zone 4, the composition of the liquid is constant (point I), and any addition of pure solvent will dissolve a constant quantity of solid at a fixed proportion of API and co-former,

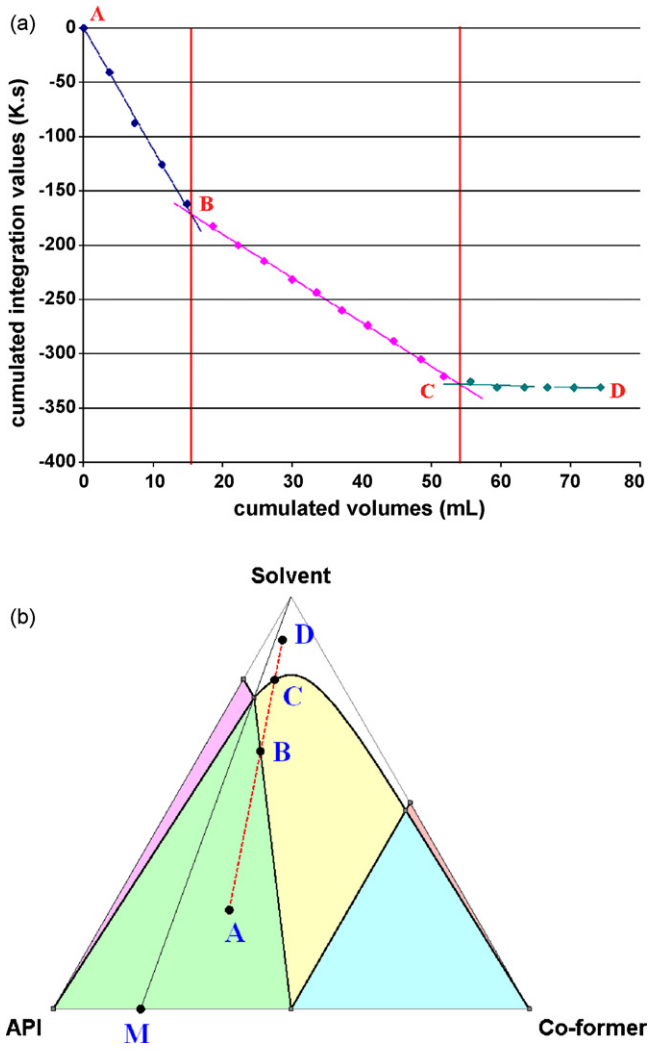

Fig. 3. (a) Changes in slope corresponding to different zones of the diagram. (b) Dilution trajectory during a typical experiment.

given by the point M. Therefore the dissolution heat per ml of added pure solvent will remain constant between A and B.

Between the points B and C, the entire quantity of solid API has already dissolved, therefore only the cocrystal will dissolve under the addition of further solvent. The heat of dissolution is that of the pure cocrystal.

After point C, all solids have dissolved, therefore there is only a negligible heat of mixing of pure solvent in the solution.

The point at which changes in the slopes occur in the cumulated (heat area) plot versus volume correspond to the intersection points B and C.

4. Results and discussion

4.1. Experimental results

4.1.1. Characterisation of the cocrystal

The API, glutaric acid and cocrystal were analyzed by XRPD, DSC, single crystal analysis and FTIR. Several techniques have been employed because of the cocrystal-salt continuum (Aakeröy et al., 2007; Park et al., 2007).

X-ray powder data confirm that a new species has been formed with a powder pattern distinct from the acid or API. DSC data confirm that the new species is a distinct entity with a single congruent melting point. Although the cocrystal melts at a temperature very close to the API, its enthalpy of fusion is far greater. FTIR analysis of the cocrystal shows a carbonyl band at 1674 cm^{-1} corresponding to the API linked by hydrogen bond (F. Debu, SA internal report.

In addition, single crystal analysis was performed internally within Sanofi Aventis and the cocrystal structure was determined (M.A. Perrin, SA internal report). The structure shows that the API and the glutaric acid are linked through a hydrogen bond network. The extent of the proton transfer between one of the carboxylic groups from the glutaric acid and a tertiary amine of the API (a (C–)O...N H–bond distance of 2.66 Å is found) was experimentally determined from a difference Fourier synthesis map. The proton is unambiguously located on the carboxylic group of the glutaric acid (with an O–H distance of 0.97 Å). Furthermore a C–O distance of 1.29 Å is found. Both are clear indications of the cocrystal nature of the solid compound.

The API has a p*K*a of 5.4 and first p*K*a of glutaric acid in water is 4.3. According to the literature (Park et al., 2007), a p*K*a difference of less than 2 units most likely leads to cocrystal formation.

Thus the nature of this stoichiometric complex is confirmed as a cocrystal.

4.1.2. Phase diagrams

The measured solubility phase diagrams for the (API: glutaric acid) cocrystal in AcOEt, MIBK, ACTN and MTBE at 25 °C are shown in Fig. 6.

For AcOEt and MIBK, the diagrams look relatively symmetric, as the solubilities of the API and co-former in these solvents are quite similar. The API is much less soluble than the co-former in ACTN or MTBE and the diagrams are very asymmetric. In the case of MTBE, the top portion of the cocrystal solubility curve appears to have disappeared.

MIBK and AcOEt appear to be the best solvents for crystallizing the cocrystal species. It may be noted from Fig. 6 that the triangular diagram for ACTN, although not particularly symmetric, still includes the 1:1 stoichiometric ratio in zone 1. No issues were observed in crystallizing the cocrystal from this solvent.

4.2. Discussion

4.2.1. Modeling the phase diagram

In order to model the phase diagram presented in Fig. 1, the following equilibria must be determined:

- The equilibrium between pure API (or pure co-former) and solution, e.g. the line separating zone 2 and 6 (or 3 and 6 for the pure co-former)
- The equilibrium between cocrystal and solution, e.g. curve separating zone 6 and 1.

It should also be noted that we neglect the contribution of the API/co-former in solution (Rodriguez-Hornedo et al., 2006b), due to the difficulty in incorporating it into the subsequent thermodynamic treatment. We will show that, for the present case, it has little impact.

To improve readability, the letters A and B have been used in the explanation below to represent cocrystal and co-former.

For the API (or co-former solid) – solution equilibrium: it may be assumed, as a first approximation, that a small addition of A in a pure solution of B does not change its solubility at all:

$$x_A = x_A^* \qquad x_B = x_B^* \qquad (1a,b)$$

x denotes the molar fraction and the * corresponds to the binary solubility of the pure component at a fixed temperature.

For the cocrystal/solution equilibrium: we use the description established by N. Rodriguez-Hornedo (Rodriguez-Hornedo et al.,

Table 2
Comparison of values of constants calculated and obtained through experiments for the different solvents.

Solvent	$x^*_{\text{co-former}}$	x^*_{API}	K_{app} calculated from gammas and experimental data	R^2	K_{app} calculated from MIBK modelling
AcOEt	0.082	0.047	2.33E−04	0.968	2.95E−04
MIBK	0.065	0.049	2.44E−04	0.984	
ACTN	0.037	0.0075	1.42E−05	0.947	2.13E−05
MTBE	0.12	0.0082	5.69E−05	0.829	7.54E−05

2006b) at the experimental temperature:

$$aA_{\text{solution}} + bB_{\text{solution}} \leftrightarrow A_aB_{b_{\text{cocrystal}}} \quad (2)$$

a and b are the stoichiometric coefficients.

The Gibbs mass action law applies to this equilibrium, therefore:

$$a\mu_A + b\mu_B = \mu_{A_aB_b} \quad (3)$$

where μ_A, μ_B, μ_{AaBb} refer to the chemical potential of the species A, B, and A_aB_b respectively.

If we choose the thermodynamic reference state as the most stable crystal form, then:

$$\mu_A = \mu_A^0 + RTLn(a_A)$$
$$\mu_B = \mu_B^0 + RTLn(a_B) \quad (4a,b,c)$$
$$\mu_{A^aB^b} = \mu^0_{A^aB^b}$$

where the index ° refers to the reference state.

Eq. (3) becomes:

$$RTLn(a_A^a a_B^b) = \mu^0_{A^aB^b} - (a\mu_A^0 + b\mu_B^0) = \Delta G^f \quad (5)$$

$$K = a_A^a a_B^b = e^{\frac{-\Delta G^f}{RT}} \quad (6)$$

ΔG^f represents the cocrystal free enthalpy of formation and K the "true" complexation constant, which is independent from the solvent.

Now we can substitute in the activity coefficients γ for A and B, which describe the molecule/solvent interactions. If we assume that the API and co-former are sufficiently diluted so that the activity coefficients are constant.

$$a_A = \gamma_A x_A$$
$$a_B = \gamma_B x_B \quad (7)$$

$$K = a_A^a a_B^b = (\gamma_A x_A)^a (\gamma_B x_B)^b \quad (8)$$

Eq. (8) is very close to the model proposed by N. Rodiguez-Hornedo (Rodriguez-Hornedo et al., 2006b). However we use the activities instead of the concentrations, which have the advantage of being solvent independent.

The apparent constant in each particular solvent, K_{app}, may be defined as:

$$K_{\text{app}} = \frac{K}{{\gamma_A}^a {\gamma_B}^b} \quad (9)$$

The apparent constant in a given solvent is related to the "true" constant by the activity coefficients of the API and co-former in this solvent (Eq. (9)).

Finally, for a given solvent the cocrystal/solution equilibrium is given by:

$$x_A{}^a x_B^b = K_{\text{app}} \quad (10)$$

If Eq. (1a,b) and Eq. (10) are plotted on a triangular diagram for a 1:1 cocrystal (e.g. $a = b = 1$), we obtain the theoretical phase diagram presented as shown in Fig. 4.

On this diagram, the curve corresponding to Eq. (10) is symmetric for $a = b = 1$. The asymmetry of the diagram is introduced by the difference in solubility of API and co-former.

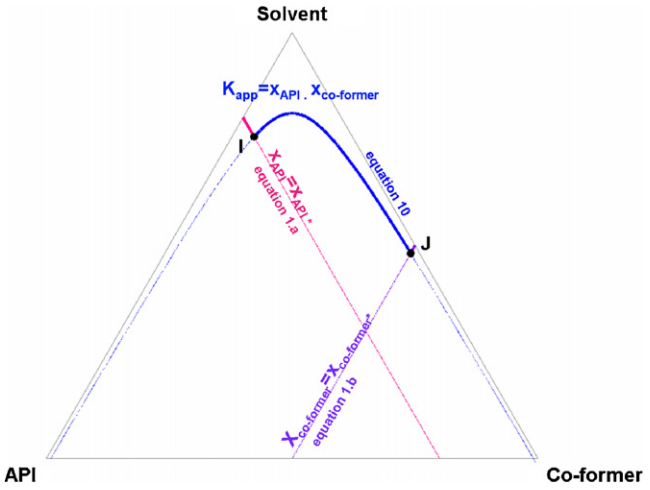

Fig. 4. Steps to construct lines and curve of a ternary diagram.

K_{app} determination from experimental data: K_{app} may be determined from experimental data by rearranging Eq. (10) thus:

$$x_A^a = \frac{K_{\text{app}}}{x_B^b} \quad (11)$$

Therefore, plotting ${x_A}^a$ versus $1/{x_B}^b$ only for the curved part of the phase diagram between points I and J), K_{app} to be calculated (the slope of the line). Fig. 5 illustrates the experimental data and the least squares regression lines, constrained to pass through the origin and calculated using Excel. K_{app} values are listed in Table 2. Experimental values for K_{app} range over approximately one order of magnitude. The R^2 coefficients are close to 1 for AcOEt, MIBK, ACTN, and a little lower but still acceptable for MTBE (the MTBE phase diagram is very asymmetric and therefore difficult to acquire).

4.2.2. Use of phase diagrams in understanding the crystallization of cocrystals

Based on the construction of triangular phase diagram, several parameters, relevant from a processing point of view, may be discussed. Crystallization is often carried out by cooling a solution.

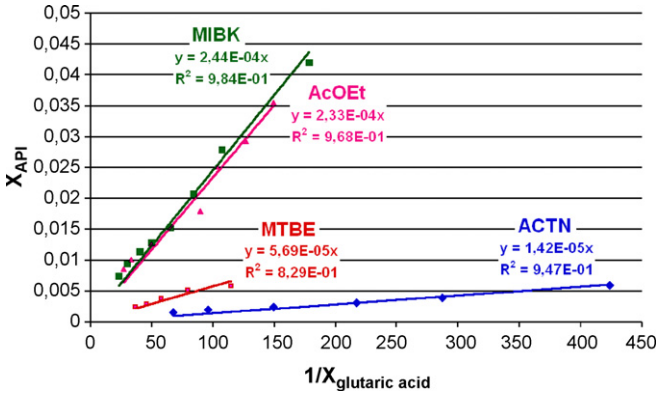

Fig. 5. $1/x$ (acid) versus x (API) for AcOEt, MTBE, MIBK and ACTN at 25 °C.

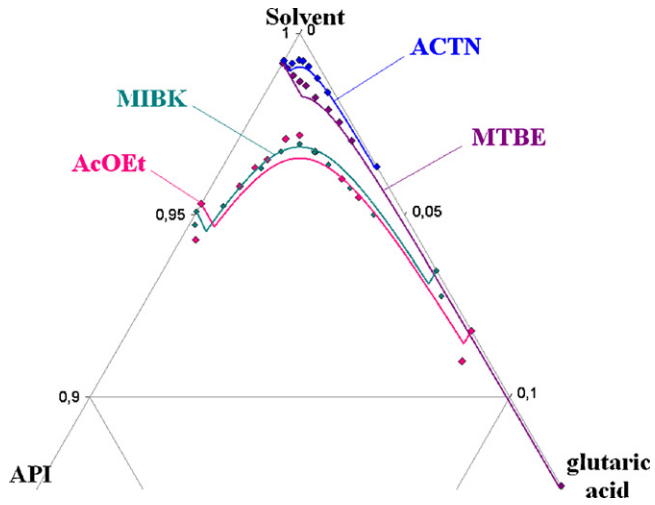

Fig. 6. Modelling (solid line) and experimental data (points) for different solvents.

The effect of the temperature is illustrated in Fig. 7 which displays two isothermal cuts of the phase diagram. At high temperature, API, co-former and cocrystal are more soluble. Therefore, in order to perform the crystallization one has to chose a process composition which is soluble at high temperature and in the cocrystal zone at low temperature. In Fig. 7 the composition represented by the circle is soluble at high temperature but insoluble at low temperature. The crystallization yield will depend, as for a conventional crystallization, on the gradient of solubility with temperature.

Depending on the relative solubility of the API, co-former and cocrystal, several types of triangular diagrams may be observed:

- When the solubility of the API and co-former are of the same order of magnitude, and higher than the cocrystal solubility (Fig. 8a), zone 1 is relatively symmetric, that is to say it is present in both the left and right sides of the diagram. In such a case, it is possible to isolate the cocrystal from the solvent using a stoichiometric ratio of API and co-former.
- If the solubility of the API is significantly reduced, (Fig. 8b) then zone 1 will shrink and move in the right side of the diagram. It is still possible to isolate the cocrystal from the solvent, but an excess of co-former should be used. Therefore, solvents exhibiting asymmetric diagrams (Fig. 8b) may still be used to crystallize the cocrystal and may present further advantages over systems with a more symmetrical phase diagram, for example in terms of purity, crystal shape or ease of drying. It should be noted that knowledge of the phase diagram is key to selecting a suitable solvent and conditions.
- If the solubility of the API is further reduced (Fig. 8c), then zone 1 completely disappears. It is not possible to crystallize the cocrystal in this solvent. If the cocrystal is added to this solvent it will dissolve and the individual components will eventually crystallize separately.

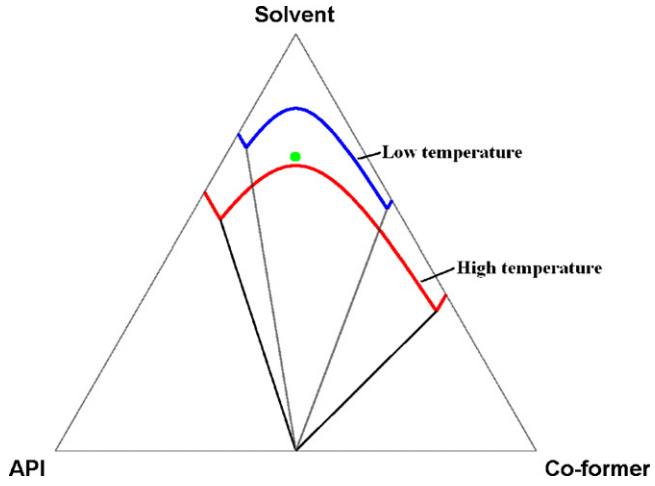

Fig. 7. Effect of temperature on the phase diagram.

It should be noted that the situations described by Fig. 8b and c may explain the difficulty observed in scaling-up some cocrystals obtained by co-grinding. Indeed, the co-grinding process is always possible, at least from a thermodynamic point of view, whereas zone 1 could be very narrow or even absent in the ternary phase diagram

5. Prediction of Phase diagram

As already mentioned, in order to choose the best solvent for cocrystallization, knowledge of phase diagrams is required. Determination of multiple phase diagrams generally requires significant experimental effort. Any prediction method, therefore, will be useful. In this section we will explain, how, from knowing the phase diagram in a given solvent we can predict the phase diagram in other solvents, using a minimal amount of additional experimental data.

5.1. Theory

The solubility of the pure component A (or B) in a solvent is related to their ideal solubility by the activity coefficient, according a well known relationship (for instance Schuffenecker et al., 1991):

$$\gamma_A = \frac{x_A^i}{x_A^*} \tag{12}$$

By combining Eqs. (9) and (12), we can eliminate the ideal solubility (Roman numerals I and II stand for two different solvents):

$$K_{app}^{II} = K_{app}^{I} \frac{(\gamma_A \gamma_B)^I}{(\gamma_A \gamma_B)^{II}} = K_{app}^{I} \frac{(x_A^* x_B^*)^{II}}{(x_A^* x_B^*)^I} \tag{13}$$

Eq. (13) aids in defining an experimental strategy:

- Measure the solubility of API and co-formers in a set of solvents;
- Chose the "easiest" solvent, namely the solvent where both components have the greatest solubility;
- Measure the phase diagram and determine K_{app} in this reference solvent;
- Calculate K_{app} in the other solvents according Eq. (13).

5.2. Comparison to experimental data

In this section we will illustrate the strategy proposed above and demonstrate that we can deduce the diagrams of API and glutaric acid (e.g. co-former) in MTBE, ACTN and AcOEt from the MIBK phase diagram.

The solvents AcOEt, MTBE and ACTN have been chosen in order to see if this model is valid for symmetrical and especially for asymmetrical diagrams (i.e.: diagrams with noticeable difference in solubilities between the API and co-former). Fig. 6 illustrates the experimental results, on which the theoretical curves have been superimposed; the theoretical curves have been calculated using the value of K from the MIBK experimental data.

Table 2 and Fig. 9 compare values of K_{app} obtained by regression and modelling from MIBK data (via Eq. (13)). The agreement

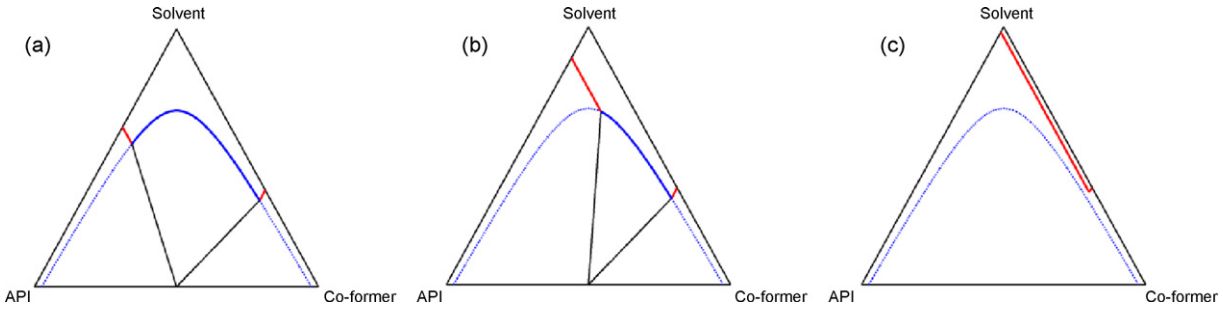

Fig. 8. Different types of phase diagrams for cocrystals (describing only the cocrystal zones and solubility curves).

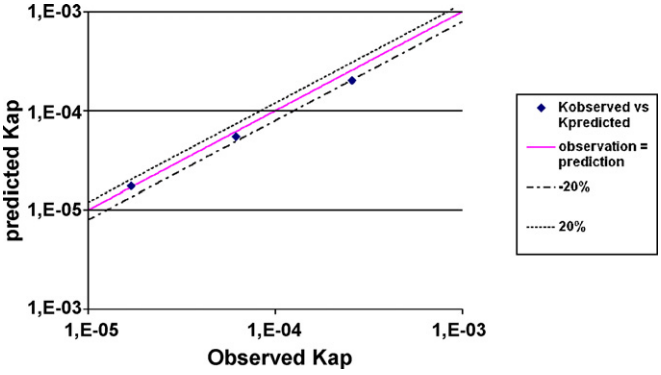

Fig. 9. Comparison of K_{app} observed by experiment and K_{app} calculated from the model using MIBK as the solvent.

between the two techniques is good. All the predicted K_{app} values are within the 20% error limits.

The experimental points "I" and "J" for MIBK and AcOEt correspond to slightly higher solubility than predicted. This may be explained by the formation of an API/glutaric acid complex in solution. The effect, however, does not grossly affect the accuracy of the experiment.

6. Conclusions

Scaling up the cocrystallization requires knowledge of the ternary solvent-API-co-former diagrams. In order to choose the best solvent for crystallization at an industrial scale, numerous solvents have to be tested, which, in the absence of an efficient method, may be long and tedious. We propose to use the DITA method, to determine a first precise phase diagram of the cocrystal in a particular solvent chosen as one in which all the individual components have reasonable solubility (information usually available at an early stage in development). This method still requires several days for an experiment but little human resources. Based on the data generated, only the solubility of the pure components is necessary to calculate the phase diagram for any other solvent. One limitation of this method is the inability to model API/co-former complexation in solution (Rodriguez-Hornedo et al., 2006b). It does, however, provide sufficient accuracy to determine the relevant process conditions for each solvent.

Clearly, once a solvent has been chosen for the industrial process, the DITA method may be used once more to refine the predicted phase diagram.

Acknowledgements

The authors acknowledge Dr M.A. Perrin, Dr F. Debu of sanofi-aventis for crystallographic and infra red data and Dr M. Bauer from sanofi-aventis from fruitful scientific discussions. The authors also acknowledge Prof. Gerard Coquerel at the University of Rouen (France) for the advices and help concerning DITA equipment.

References

Aakeröy, C.B., Fasulo, M.E., Desper, J., 2007. Cocrystal or salt: does it really matter? Mol. Pharm. 4, 317–322.
Aakeröy, C.B., Hussain, I., Desper, J., 2006. 2- Acetaminopyridine: a highly effective cocrystallizing agent. Cryst. Growth Des. 6, 474–480.
Aakeröy, C.B., Salmon, D.J., 2005. Building co-crystals with molecular sense and supramolecular sensibility. Cryst. Eng. Commun. 7, 439–448.
Bak, A., Gore, A., Yanez, E., Stanton, M., Tufekcic, S., Syed, R., Akrami, A., Rose, M., Surapaneni, S., Bostick, T., King, A., Neervannan, S., Ostovic, D., Koparkar, A., 2008. The co-crystal approach to improve the exposure of a water-insoluble compound: AMG 517 sorbic acid co-crystal characterization and pharmacokinetics. J. Pharm. Sci. 97, 3942–3956.
Bishop, R., Alshahateet, S.F., Nakano, K., Craig, D.C., Harris, K.D.M., Scudder, M.L., 2004. Co- crystalline hydrogen bonded solids based on the alcohol-carboxylic acid-alcohol supramolecular motif. Cryst. Eng. Commun. 6, 5–10.
Braga, D., Grepioni, F., 2005. Making crystals: a green route to crystal engineering and polymorphism. Chem. Commun. 29, 3635–3645.
Collet, A., Jacques, J., Wilen, S.H., 1981. Enantiomers Racemates and Resolution. Wiley, New York.
Chiarella, R.A., Davey, R.J., Peterson, M.L., 2007. Making co-cocrystals: the utility of ternary phase diagrams. Cryst. Growth Des. 7, 1223–1226.
Ito, K., Sekiguchi, K., 1966. Studies on the molecular compounds of organics medicinals, Application of the solubility product principle and consideration by the phase rule to the solubility phenomena of the molecular compound of sulphanilamide and sulfathiazole. Chem. Pharm. Bull. 14, 255–262.
Jones, W., Trask, A.V., Motherwell, W.D.S., 2006. Physical stability enhancement of theophylline via cocrystallization. Int. J. Pharm. 320, 114–123.
Jones, W., Trask, A.V., Motherwell, W.D.S., 2005. Pharmaceutical cocrystallization: engineering a remedy for caffeine hydratation. Cryst. Growth Des. 5, 1013–1021.
Jones, W., Shan, N., Toda, F., 2002. Mechanochemistry and co-crystal formation: effect of solvent on reaction kinetics. Chem. Commun. 20, 2372–2373.
Li, Y., Chow, P.S., Tan, R.B.H., Black, P.S., 2008. Effect of water activity on the transformation between hydrate and anhydrate of carbamazepine. Org. Process Res. Dev. 12, 264–270.
Marchand, P., Lefebvre, L., Querniard, F., Cardinael, P., Perez, G., Counioux, J.-J., Coquerel, G., 2004. Diastereomeric resolution rationalized by phase diagrams under the actual conditions of the experimental process. Tetrahedron: Asymmetry 15, 2455–2465.
Mc Namara, D.P., Childs, S.L., Giordano, J., Iarriccio, A., Cassidy, J., Shet, M.S., Mannion, R., O'Donnell, E., Park, A., 2006. Use of glutaric acid cocrystal to improve oral bioavailability of a low solubility API. Pharm. Res. 23, 1888–1897.
Park, A., Childs, S.L., Stahly, G.P., 2007. The salt-cocrystal continuum: the influence of crystal structure on ionization state. Mol Pharm. 4, 323–338.
Remenar, J.F., Morisette, S.L., Peterson, M.L., Moulton, B., MacPhee, M.J., Guzman, H.R., Almarsson, O., 2003. Crystal engineering of novel co-crystal of a triazole drug with 1, 4-dicarboxylic acids. J. Am. Chem. Soc. 125, 8456–8457.
Rodriguez-Hornedo, N., Nehm, S.J., Seefeldt, K.F., Pagan-Torres, Y., Falkiewicz, C.J., 2006a. Reaction crystallization of pharmaceutical molecular complexes. Mol. Pharm. 3, 362–367.
Rodriguez-Hornedo, N., Nehm, S.J., Rodriguez-Spong, B., 2006b. Phase solubility of cocrystals are explained by solubility product and solution complexation. diagrams. Cryst. Growth Des. 6, 592–600.
Schuffenecker, L., Bouchy, M., Foucault, J.F., Martel, L., Proust, B., Scacchi, G., 1991. Thermodynamique et cinétique chimiques. Technique et Documentation-Lavoisier Paris.
Smith, G., Baldry, K.E., Byriel, K.A., Kennard, C.H.L., 1997. Molecular cocrystals of carboxylic acids, The utility of urea in structure making with carboxylic acids and the crystal structures of a set of six adducts with aromatic acids. Aust. J. Chem. 50, 727–736.
Variankaval, N., Wenslow, R., Murry, J., Hartman, R., Helmy, R., Kwong, E., Clas, S.-D., Dalton, C., Santos, I., 2006. Preparation and solid-state characterization of nonstoichiometric cocrystals of a phosphodiesterase- IV inhibitor and L-tartaric acid. Cryst. Growth Des. 6, 690–700.

York, P., Bladgen, N., de Matas, M., Gavan, P.T., 2007. Crystal engineering of active pharmaceutical ingredients to improve solubility and dissolution rates. Adv. Drug Delivery Rev. 59, 617–630.

Zaworotko, M.J., Bailey Walsh, R.D., Bradner, M.W., Fleischman, S.G., Morales, L.A., Moulton, B., Rodriguez-Hornedo, N., 2003a. Crystal engineering of the composition of pharmaceutical phases. Chem. Commun. 2, 186–187.

Zaworotko, M.J., Fleischman, S.G., Kuduva, S.S., McMahon, J.A., Moulton, B., Bailey Walsh, R.D., Rodriguez-Hornedo, N., 2003b. Crystal engineering of the composition of pharmaceutical phases: multiple-component crystalline solids involving carbamazepine. Cryst. Growth Des. 3, 909–919.

Zaworotko, M.J., Vishweshwar, P., McMahon, J.A., Peterson, M.L., Hickey, M.B., Shattock, T.R., 2005. Crystal engineering of pharmaceutical co-crystals from polymorphic active pharmaceutical ingredients. Chem. Commun. 36, 4601–4603.

Zaworotko, M.J., Moulton, B., 2001. From molecules to crystal engineering: supramolecular isomerism and polymorphism in network solids. Chem. Rev. 101, 1629–1658.

Zhang, G.G.Z., Henry, R.F., Borchardt, T.B., Lou, X., 2006. Efficient co-crystal screening using solution-mediated phase transformation. J. Pharm. Sci. 96, 990–995.